Surface & Coatings Technology 304 (2016) 553–559

Contents lists available at ScienceDirect

Surface & Coatings Technology

journal homepage: www.elsevier.com/locate/surfcoat

Hard yet tough V-Al-C-N nanocomposite coatings: Microstructure, mechanical and tribological properties

Zhenyu Wang [a,b], Xiaowei Li [a], Xin Wang [a], Sheng Cai [a], Peiling Ke [a,*], kepl @nimte.ac.cn;, Aiying Wang [a,*]

[a] Key Laboratory of Marine Materials and Related Technologies, Zhejiang Key Laboratory of Marine Materials and Protective Technologies, Ningbo Institute of Materials Technology and Engineering, Chinese Academy of Sciences, Ningbo 315201, China
[b] University of Chinese Academy of Sciences, Beijing 100049, China

ARTICLE INFO

Article history:
Received 30 May 2016
Revised 20 July 2016
Accepted in revised form 21 July 2016
Available online 22 July 2016

Keywords:
Nanocomposite
Hard yet tough
sp^2-riched amorphous carbon
Wear resistance
Lubrication

ABSTRACT

Hard coatings have been widely used in industrial applications as wear-resistant coatings, but are prone to failure due to the high intrinsic brittleness. In order to improve toughness without significantly sacrificing hardness, here we designed the V-Al-C-N nanocomposite coatings, and the microstructures consisting of V-based nanocrystalline hard phases and sp^2-riched amorphous carbon soft phases were successfully manipulated by sputtering V_2AlC target under various N_2 flow rates. Results indicated that the coating hardness was almost independent on the N_2 flow rate and maintained around ~30 GPa as changing N_2 flow rate from 5 to 20 sccm, while the toughness was significantly improved, and the high H/E ratio of 0.11 and elastic recovery of 69% could be obtained, respectively. In addition, the V-Al-C-N nanocomposite coatings showed low wear rate ($<1.5\times10^{-16}$ m^3/Nm) under a normal load of 10 N. The hard yet tough characteristic and high wear resistance for the deposited coatings were attributed to the special nanocomposite microstructures as well as the synergistic lubricant effect derived from both sp^2-riched amorphous carbon and V_2O_5 Magnéli phases formed during friction stage.

1. Introduction

In the past few years, transition metal nitride or carbide hard coatings have been widely studied for various applications [1–3]. However, due to the rapid development of high-speed or heavy-duty manufacturing processes and tribologically stressed components application, the design and fabrication of the required multi-functional hard coatings with the combined high hardness, good toughness, wear resistance and so on still remain a challenge [4]. Embedding the nanocrystalline phase into amorphous matrix to form the nanocomposite structure provides a promising way to tailor the coating properties to a specific desired value and thus satisfy the required properties [5–7].

Since the superhard (>40 GPa) Ti–Si–N coatings based on nanocomposite structure comprising TiN nano-crystallites and a grain boundary phase of amorphous SiN_x was obtained [8], many researches [9,10] were focused on how to improve the coating hardness by adjusting interface, oxygen content or the amount of amorphous phase in Ti-Si-N or other systems, such as Cr-Si-N [11], Ti-B-N [12], Cr-B-N [13] and so on. Despite the superhardness, their friction coefficients are rather high [14,15] thus hinder its application in dry machining. Recently, V-based hard coating has aroused wide interest due to its lower friction coefficient (<0.4) over a wider temperature range (293–993 K) than the traditional Ti or Cr-based coatings [16,17]. Ge et al. [18] successfully prepared the V-Si-N nanocomposite coatings with high hardness (>30 GPa) and low friction coefficient (~0.4), but the severe wear still occurred under the normal load of 10 N during dry sliding condition due to its poor toughness. Pei et al. [19] also found that the toughness played a key role in the wear resistance and the hard coating with high toughness was usually followed by the superior wear resistance property. However, it is difficult to obtain the coatings with high toughness without sacrificing superior hardness. The combination of the hard nanocrystalline phase (10–20 nm) with a soft matrix (2–10 nm) such as TiAlCN/a-C [20], ZrN/Cu [21] or SiC/Ni [22] has been proved to be an effective way to meet hard yet tough properties suggested by Voevodin et al. [23]. The crystallite size of the hard phase was maintained at the nanometric level to guarantee the hardness, while the second soft phase provided ductility [24]. Previous studies [4,24] indicated that amorphous carbon existed in the grain boundary and it can not only improve the coating hardness and toughness but also decrease the friction coefficient and further enhance the wear resistance. Many researchers have synthesized the hard yet tough carbon-composited coatings for tribological applications, such as Ti–N–C [25], Cr–C–N [26,27], Ti-Al-C–N [28], and Ti-Si-C–N [29]. However, there is still a difficulty and challenge to control the structures of these nanocomposite coatings with the combination of high hardness, good toughness and wear resistance by a facile technique over large area. Especially, the nanocomposite coatings composed of V-based nanocrystalline hard phase and amorphous carbon lubricious phase have not yet been reported in detail.

* Corresponding authors.
E-mail address: aywang@nimte.ac.cn (A. Wang).

http://dx.doi.org/10.1016/j.surfcoat.2016.07.061
0257-8972/

Table 1
Chemical composition of as-deposited V-Al-C-N coatings determined by XPS.

Sample	Chemical composition (at%)					(C + N)/(V + Al) ratio	N/C + N	Thickness (nm)
	O	V	Al	C	N			
S1	6.08	39.69	8.29	45.94	–	1.01	–	2000
S2	4.95	25.72	12.08	32.73	24.53	1.51	0.43	1950
S3	4.69	23.58	12.09	33.22	26.43	1.67	0.44	2220
S4	4.37	24.57	12.95	29.61	28.53	1.55	0.49	2230
S5	3.76	24.44	11.58	29.94	30.29	1.67	0.50	2150

In the present work, V-Al-C-N nanocomposite coatings were prepared by reactive sputtering from a V_2AlC compound target under Ar/N_2 gas mixtures. Because of the stronger chemical binding of nitrogen relative to carbon, to vanadium ions [30] and the limited carbon solubility in the lattice of metal nitrides, the nanostructure as well as the formation and content of amorphous carbon were controlled by varing the nitrogen flow rate. The composition and microstructure of the coatings and the related mechanical and tribological properties are investigated. The optimization of the nanocrystalline and amorphous phases was carried out by controlling the nitrogen flow rate to achieve a combination of high hardness, good toughness and wear resistance properties.

2. Experimental details

V-Al-C-N coatings were prepared by a hybrid ion beam deposition system [31] consisting of a circular DC magnetron sputtering and a linear anode-layer ion source (LIS). P-type Si (100) wafers and mirror-finished high speed steel (HSS) with a dimension of 15 mm × 15 mm × 3 mm were used as substrates. Prior to deposition the substrates were ultrasonically cleaned in acetone and ethanol for 15 min, respectively. To improve the adhesion strength of the coating to substrate, all the substrates were sputter-cleaned for 30 min using Ar ions generated by LIS to remove the contaminants of surface, and then a Ti interlayer with thickness of ~0.25 μm was introduced. After that, V-Al-C-N coatings were deposited in Ar/N_2 gas mixtures, at a base pressure of 2.0×10^{-3} Pa and deposition pressure of 0.5 Pa to 0.9 Pa. The Ar flow rate of 70 sccm was kept constant for all deposition process, while the N_2 flow rate was changed from 0 to 40 sccm to adjust the coating composition. The V-Al-C-N coatings were labeled S1 to S5 according to the used deposition parameters. The substrate temperature and distance of target to substrate were kept constant at ~250 °C and 160 mm, respectively. The substrate bias voltage of −150 V with a frequency of 350 kHz and reverse time of 1.1 μs was applied.

The microstructure of the coatings was investigated by glancing incident x-ray diffraction (GIXRD), scanning electron microscopy (SEM), Raman spectroscopy and cross-sectional transmission electron microscopy (TEM). The GIXRD measurements were performed on a Bruker D8 Advance diffractometer (Cu-Ka radiation) with a glancing incident angle (0.5°). The cross-sectional morphology of the coatings was examined by a Hitachi S4800 high-resolution field emission SEM. Raman spectroscopy (In Via-reflex, Renishaw) equipped with a 60 mW He–Ne laser of 532 nm exciting wavelength was used to evaluate the substructures of nitride and free carbon in the deposited coatings. Cross-sectional TEM studies were performed on a FEI Tecnai G2 TF20 system operated at an accelerating voltage of 200 kV. The specimens for plan-view TEM examination were prepared through mechanical polishing and ion milling. Chemical bonding state and compositions analysis through x-ray photoelectron spectroscopy (XPS) was performed in a Kratos Axis ULTRA DLD XPS system, using a monochromatized Al (Ka) x-ray source with photon energy, $h\nu = 1486.6$ eV. The graphite C 1s position at 284.6 eV was used as reference for the energy calibration and a Shirley-type background subtraction was used in data analysis. For each sample, two XPS tests were made to estimate the average chemical compositions and the XPS signals were taken at about 500 nm depth into the coating.

Mechanical properties were measured by a MTS Nanoindenter G200 tool in a continuous stiffness measurement mode using a Berkovich diamond tip. Hardness and.

Young's modulus were determined using the Oliver-Pharr method. The characteristic hardness was chosen in a depth of around 1/10 of the coating thickness, where the measured value was not affected by the substrate. Six replicate indentations were done for each sample. Tribological behavior was evaluated by reciprocating ball-on-plate dry sliding tests against Al_2O_3 balls with a diameter of 6 mm on a universal tribometer (RTEC Instruments). The sliding speed and frequency were set at 0.02 m/s and 2 Hz, respectively. All tests were conducted under a load of 10 N at the ambient temperature (~293 K) and a relative humidity of 50–60%. The total sliding time was 3600 s. After tests, the wear track profiles were measured by the surface profilometer. The wear rates were evaluated as volume per sliding distance per load. The morphology of the wear tracks was examined by the FEI Quanta FEG 250 SEM, while the chemical species was probed by the Micro-Raman spectroscopy mentioned above, which was equipped with a 50× objective lens to locate the regions of interest.

3. Results and discussion

3.1. Composition and phase structure

The Chemical composition of the deposited V-Al-C-N coatings is given in Table 1. It shows that N content and N/(C + N) ratio increase monotonically with increasing the N_2 flow rate. For the V-Al-C coating (S1), the C/(V + Al) ratio is around 1, while the (N + C)/(V + Al) ratio increases significantly and varies in a narrow range, from 1.51 to 1.67, when the N is incorporated, implying the controlled composition of introduced N content. It should be noted that there is low content of oxygen contamination presented in all samples due to the possible low base vacuum degree.

The phase evolution of the V-Al-C-N coatings was examined using GIXRD. As shown in Fig. 1, the V-Al-C coating is composed of face-centered cubic (fcc) (V, Al)C phase with (111) preferred orientation at the diffraction peak 2θ of approximately 38.24°, which is similar to the case of Ti-Al-C-N coatings [32], but the lattice parameter for fcc-(V, Al)C is smaller than the ideal fcc-VC phase (PDF#65-8825 VC) because of the partial replacement of V by Al atoms. For the V-Al-C-N coatings, it still exhibits the face-centered cubic structure, but the incorporation of N into V-Al-C coatings leads to the shift of (111) peak toward lower diffraction angle, which attributes to the changes in the chemical

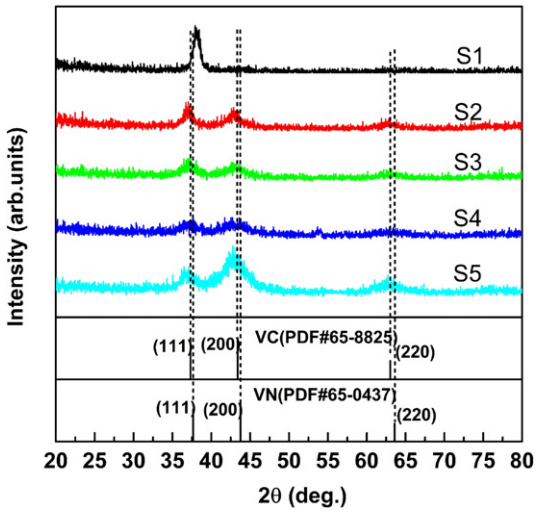

Fig. 1. GIXRD patterns of the V-Al-C-N coatings deposited under different N_2 flow rate.

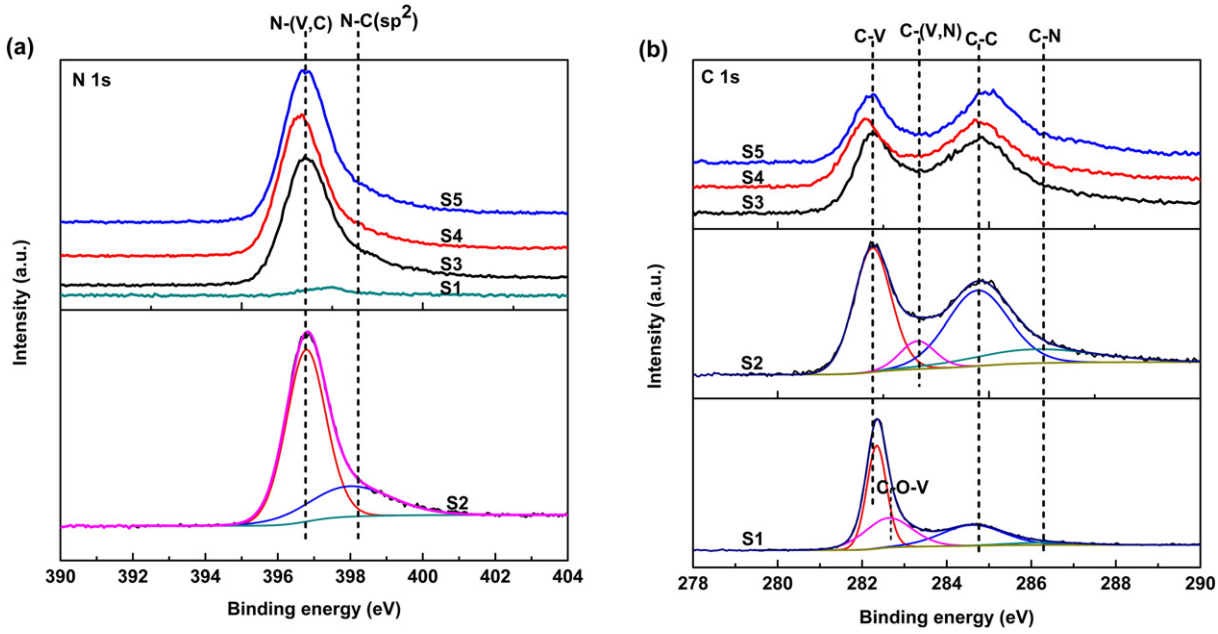

Fig. 2. XPS spectra of V-Al-C-N coatings deposited under different N_2 flow rates: (a) N 1s; (b) C 1s.

composition and the residual stress of the coatings [33]; in addition, the other two peaks located at $2\theta = 43.48°$ and 63.52° are assigned to (200) and (220) reflections, respectively. Because the lattice constant value of the VC and VN phases is adjacent, it is difficult to accurately distinguish the phase constitute just by XRD analysis. Previous study [30] reported that a small amount of N could replace the C sites in the fcc-(V, Al)C lattice to form the fcc-(V, Al)(C, N). Meanwhile, the diffraction peak widths are broader with the nitrogen incorporation, revealing that nitrogen incorporation can fine the nanocrystallites.

To characterize the bonding structure of the coatings, typical high-resolution core-level XPS analyses were carried out. Fig. 2 presents the C 1s and N 1s XPS spectra of the V-Al-C-N coatings deposited at different parameters, respectively. Compared to V-Al-C coating (S1), the N 1s XPS spectra of V-Al-C-N coatings in Fig. 2a show a main peak at 396.8 eV and a shoulder peak at 398.1 eV, which are assigned to N—(V, C) and N—C (sp [2]) bonds, respectively [34,25]. These results indicate the successive substitution of nitrogen into carbon in (V, Al) C and linkage between the substituted carbon and the incorporated nitrogen with increasing incorporation of nitrogen. In the C 1s spectra (Fig. 2b), the spectra exhibit a significant variation with the increase of N_2 flow rate. For the V-Al-C coating (S1), the spectra consist of the main peak at 282.4 eV which is assigned to C—V bonds [25], and two weak peaks at higher binding energies of 282.6 eV and 284.6 eV corresponding to C—O—V and sp^2 C—C bonds [35], respectively, indicating that most of the C atoms are bonded to V atoms. But in the coating of S2–S5, the C 1s spectra are fitted into four components at 282.2 eV, 283.3 eV, 284.7 eV, and 286.1 eV, which correspond to C—V, C—(V, N), C—C, and C—N bonds [36], respectively. Especially, the fraction of C—C bonds increases with increasing the N_2 flow rate, suggesting that the fraction of amorphous carbon phase increases and become main component for coating S4 and S5.

Additional information on the phase composition of the V-Al-C-N coatings obtained using Raman spectroscopy is given in Fig. 3a. It shows that the Raman spectra could be divided into two regions. One is located from 100 to 1000 cm^{-1} due to the vibrational modes of V(C, N) compound, while the other one located from 1000 to 1800 cm^{-1} shows typical asymmetric and broad peak, indicating the emergence of amorphous carbon phase in the V-Al-C-N coatings [37]. The amorphous carbon spectra are fitted into two peaks including G peak centered at ~1550 cm^{-1} originating from all graphite-like

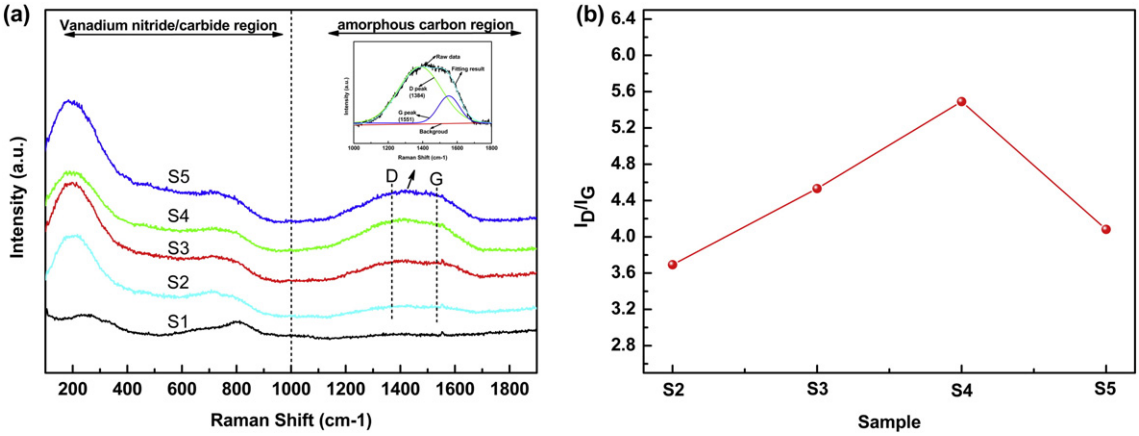

Fig. 3. (a) Raman spectra of the V-Al-C-N coatings deposited under different N_2 flow rates; (b) I_D/I_G ratio.

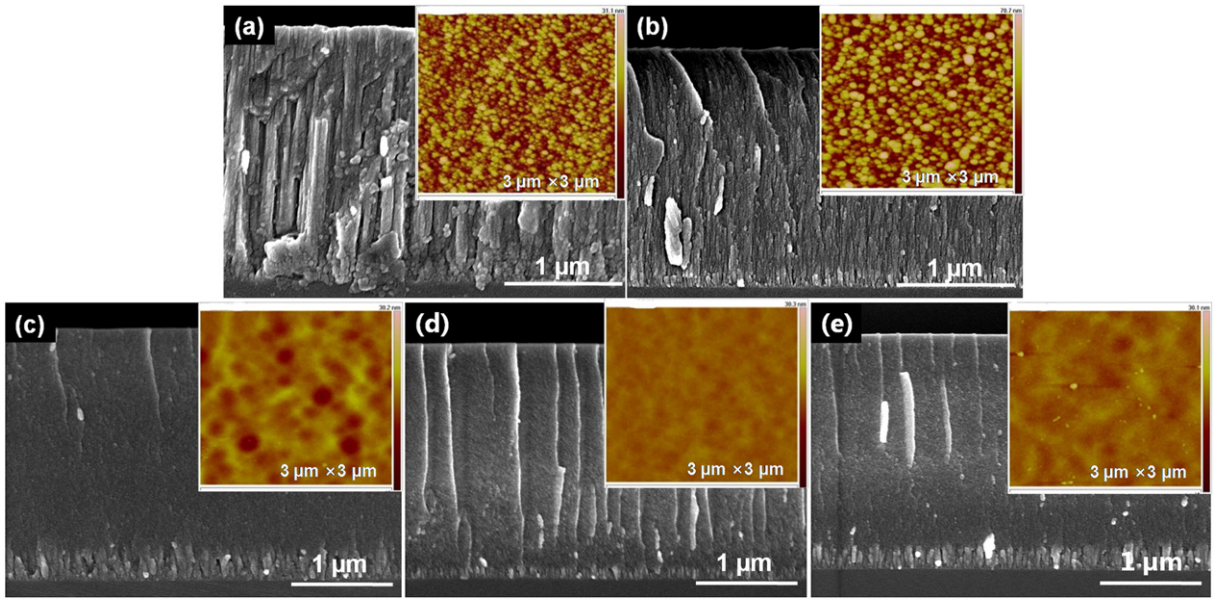

Fig. 4. Cross-sectional morphologies of the V-Al-C-N coatings deposited under different N_2 flow rates (a) S1; (b) S2; (c) S3; (d) S4; (e) S5.

sp^2 bonds and D peak centered at ~1380 cm^{-1} due to the aromatic sp^2 bonds (insert in Fig. 3a) [38]. Besides, the intensity of the D and G peaks with N_2 flow rate increases gradually, as reported for other carbonitrides [32]. Further information for carbon atomic bonds can be obtained from the intensity ratio of D peak to G peak (I_D/I_G ratio), which is given in Fig. 3b. It reveals that the I_D/I_G values of the V-Al-C-N coatings vary from 3.7 to 4.1. Taking into account that the I_D/I_G ration is closely related to the sp^2 cluster size in the coating, it can be said that incorporating N could not only promote the formation of amorphous carbon phases, but also benefit the sp^2-riched graphite-like bonds dominated in the amorphous carbon matrix [28]. Therefore, combining the XRD, XPS and Raman results, the structure of V-Al-C-N coatings is the nanocomposite structure composed of the (V,Al)(C,N) nanocrystallites and amorphous sp^2-riched carbon as well as little amount of CN_x.

3.2. Morphology and microstructure

Fig. 4 shows the fractured cross-sectional SEM micrograph of the V-Al-C-N coatings. The obvious morphology evolution of the coatings can be clearly seen following the N_2 flow rate. For the V-Al-C coating (S1), a typical columnar structure extends through the coating thickness as displayed in Fig. 4a. When the nitrogen is incorporated, the coating morphology evolves into fibrous columnar structure (Fig. 4b). Based on the aforementioned phase structure analysis, it can be concluded that the appearance of amorphous carbon probably distributed among the grain boundary inhibits the grain lateral growth. In addition, the cauliflower-like surface structure can be clearly seen by AFM (inserted in Fig. 4a and b) for the coatings S1, S2 and each cauliflower cell corresponds to the top of columnar grain. With further increasing the N_2 flow rate (coating S3), a feature-less structure is generated instead of

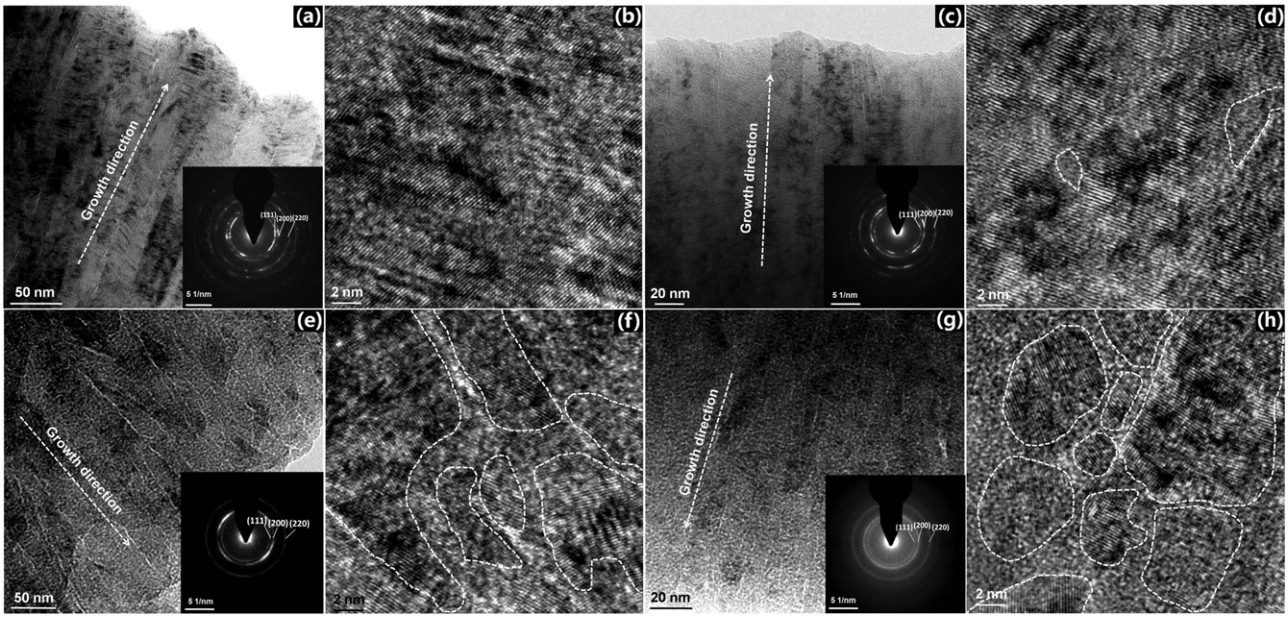

Fig. 5. Cross-sectional TEM and HRTEM images of the V-Al-C-N coatings deposited under different N_2 flow rates (a), (b) S1; (c), (d) S2; (e), (f) S4; (g), (h) S5.

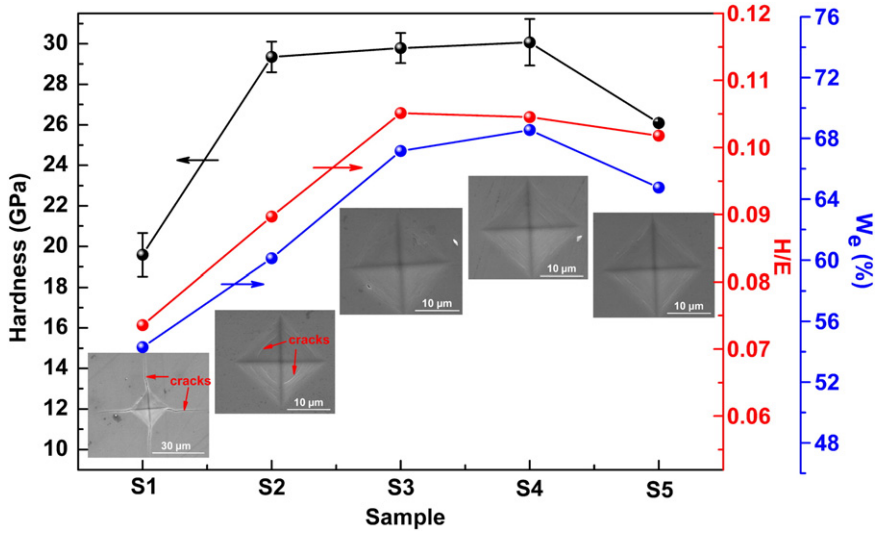

Fig. 6. Hardness, H/E ratio and elastic recovery (We) of the V-Al-C-N coatings deposited under different N_2 flow rates.

the fibrous columnar structure in S2 (Fig. 4c), which results from the increased content of amorphous carbon. For the coatings deposited under higher N_2 flow rate (S4 and S5), the surface morphology (Fig. 4d and e) stays feature-less with finer grain, the size of which cannot be evaluated from the SEM image due to the limited resolution of the used microscope.

The cross-sectional TEM observation was performed on the coating S1, S2, S4 and S5 to further investigate the detailed nanostructure development with N_2 flow rate. As shown in Fig. 5, a clear modification of the microstructure occurs by modifying the N contents of the coatings. For the N-free V-Al-C coating (Fig. 5a), it exhibits a well defined columnar microstructure with a grain width of 30-50 nm. The corresponding selective area electron diffraction (SAED) patterns in the inset of Fig. 5a shows three discontinuous rings, which are identified to be (111), (200) and (220) planes of fcc-(V,Al)C phase. This is consistent with the XRD results (Fig. 1). Moreover, high-resolution TEM (HRTEM) investigations are shown in Fig. 5b. The lattice fringes of V-Al-C coating reveal the single-crystal characteristics in each column. For the coating S2, columnar microstructure along the growth direction still exists, but it is followed by some finer grains with a width of 5–10 nm (Fig. 5c); the discontinuous SAED pattern in the inset shows three rings corresponding to the (111), (200) and (220) planes of the fcc-(V,Al)(C,N) phase. According to the HRTEM observation (Fig. 5d), amorphous phase is formed inside the column, but the nano-crystalline domains in each columnar grain still exhibit an identical lattice orientation, implying that the precipitation of amorphous phase do not block the columnar crystalline growth. As the content of amorphous phase is further increased (Fig. 5e), the columnar structure vanishes and elongated nanograins are separated by the amorphous phase. Namely, these amorphous phases completely block the continuous growth of the (V,Al)(N,C) crystallites. The near-continuous SAED pattern still shows the diffraction rings of fcc-(V,Al)(N,C), which contains strong (200) and weak (111) and (220) rings. Moreover, the HRTEM image (Fig. 5f) clearly shows the nanocomposite structure, which consists of elongated nanocrystalline (V,Al)(C,N) grains embedded in an amorphous matrix. When the nitrogen content is further increased (coating S5, as shown in Fig. 5g), the nanograins become spherical, accompanying with a further decrease of grain size. The SAED patterns in the insets exhibit continuous rings, corresponding to the finer microstructures and the increased amount of amorphous phase [39]. The HRTEM observation (Fig. 5h) further reveals the structure of the coating in which the (V,Al)(C,N) nanocrystalline is dispersed in an amorphous matrix.

3.3. Mechanical and tribological properties

Fig. 6 shows the hardness, H/E ratio and elastic recovery (W_e) of the V-Al-C-N coatings as a function of N_2 flow rate. For the N-free V-Al-C coating (S1), the results indicate that the hardness, H/E ratio and W_e are 19.59 ± 1.07 GPa, 0.07 and 54%, respectively. It should be noted that the coating hardness increases significantly and then almost

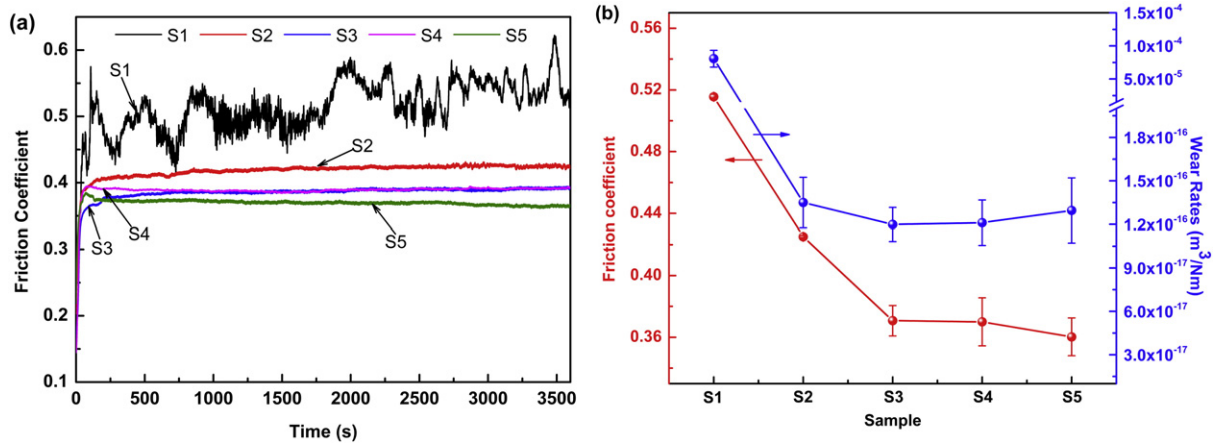

Fig. 7. (a) Friction behavior and (b) average friction coefficient and wear rates of the V-Al-C-N coatings deposited under different N_2 flow rates.

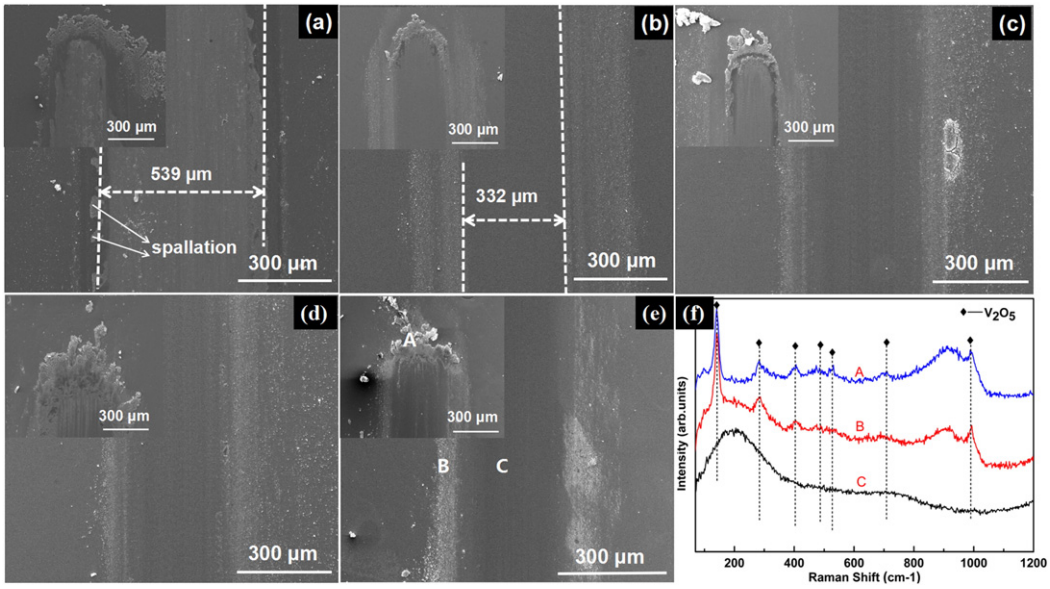

Fig. 8. SEM images of the wear track for the V-Al-C-N coatings deposited under different N_2 flow rates (a) S1; (b) S2; (c) S3; (d) S4; (e) S5 and (f) Raman results for the coating S5.

keeps constant at around 30 GPa with increasing the N_2 flow rate for the coating S2 to S4. Meanwhile, the high H/E ratio (0.11) and elastic recovery (69%) are obtained for the coating S4. Musil et al. [40] has proposed that the toughness was determined by the H/E ratio and W_e, and found that the hard coatings with enhanced resistance to cracking could be characterized by higher H/E (>0.1) and elastic recovery (W_e > 60%). Thereafter, the results here reveal that the designed V-Al-C-N nanocomposite coatings with optimized nitrogen incorporation display the enhanced toughness without sacrificing hardness. However, a slightly decreases of the hardness and elastic recovery occur with the further increase of N_2 flow rate, which might be related to the increased amorphous phase content. Indentation is a widely accepted method to measure the fracture toughness of the coatings, though the determination of the toughness is still a difficult task [41]. The insets in Fig. 6 illustrate the Vickers indentation morphology with a loaded 3 N force to assess the cracking resistance. For the V-Al-C coatings, severe radical cracks are formed along the indentation, indicating the poor toughness or adhesion to the substrate. However, for the nanocomposite V-Al-C-N coating S2, all the cracks exist inside the indentation region and there are no obvious cracks observed for the coating S3–S5, which denotes the obtained hard yet tough performance of V-Al-C-N coatings due to the formed nanocomposite structures.

Fig. 7 and Fig. 8 show the friction behavior, wear track morphology and Raman spectra of the wear debris of the different samples under the normal load of 10 N against Al_2O_3, respectively. For the V-Al-C coating S1, the friction coefficient as a function of sliding time in Fig. 7a fluctuates severely from 0.4 to 0.6 and it is worn out soon, severe wear with the wear rate of 8.06×10^{-5} m^3/Nm is obtained; Fig. 8a shows the wide wear track. The reason is that localized breaking and cracking start to form and grow during sliding when the stress exceeds a critical value of the coatings, and the columnar structure also accelerates this phenomenon. Therefore, the low hardness and poor toughness or adhesion combined with the columnar structure can account for the severe wear of V-Al-C coating under high normal load. After the nitrogen is introduced into the coatings, the friction coefficient against sliding time becomes stable after the running-in period; the average friction coefficient decreases monotonically with increasing the nitrogen composition and the lowest value of 0.36 is obtained for the coating S5. This phenomenon is related to the self-lubrication effect arising from the formation of amorphous carbon acting as a graphite-like lubricating layer [29]. The wear tracks for the coating S2 to S5 (Fig. 8b–e) seem to be very smooth and are almost free of any cracking or spalling, and the loose debris is uniformly distributed on both sides of the wear track or aggregated in the front of the wear track. In order to obtain more information about the tribological mechanisms, Raman analysis is performed on the selected area of the wear track and the wear debris for the coating S5, as illustrated in Fig. 8f. It can be seen that the V_2O_5 is present, indicating that V-based coating is oxidized to form the vanadium oxides during sliding. V_2O_5 Magnéli phase has easy slipping shear planes which can act as lubricant during tribo-process [42]. Based on the above discussion, the synergistic lubricant effect caused by the formed amorphous carbon and V_2O_5, good hardness and improved toughness result in the low friction coefficient and good wear resistance of the V-Al-C-N coatings.

4. Conclusions

The V-Al-C-N nanocomposite coatings were deposited by sputtering V_2AlC compound target under different nitrogen flow rates. The detailed composition and microstructure as well as the related mechanical and tribological properties of these coatings were evaluated. The incorporation of nitrogen decreased the grain size and promoted the formation of the sp^2-riched amorphous carbon. With increasing the nitrogen flow rates, the nanostructure of coatings evolved from columnar structure to nanocomposite structure composed of the (V,Al)(C,N) nanocrystallites and amorphous carbon and CNx. The V-Al-C-N coating with such an optimized nanocomposite structure exhibited both high hardness (>30 GPa) and good toughness (H/E > 0.1, We > 60), which contributed to the relative low friction coefficient (<0.4) and wear rate (~1.2×10^{-16} m^3/Nm). The V-Al-C-N nanocomposite coatings prepared by sputtering V_2AlC composite target with nitrogen can be a good choice to produce the wear-resistant coatings on dry machining. Our results provide a route to fabricate the coatings with high hardness and good toughness for the dry wear-resistant applications.

Acknowledgments

The research was supported by the State Key Project of Fundamental Research of China (2013CB632302), National Natural Science Foundation of China (51522106, 51375475), and Ningbo Municipal Natural Science Foundation (2015A610073). We authors sincerely thank Prof. Magnus Odén at Linköping University for helpful discussion.

References

[1] J. Musil, Hard and superhard nanocomposite coatings, Surf. Coat. Technol. 125 (2000) 322–330.
[2] M. Tkadletz, N. Schalk, R. Daniel, J. Keckes, C. Czettl, C. Mitterer, Advanced characterization methods for wear resistant hard coatings: a review on recent progress, Surf. Coat. Technol. 285 (2016) 31–46.
[3] A. Kameneva, V. Karmanov, Physical and mechanical properties of the $Ti_xZr_{1-x}N$ thin films, J. Alloys Compd. 546 (2013) 20–27.
[4] M. Stueber, P.B. Barna, M.C. Simmonds, U. Albers, H. Leiste, C. Ziebert, H. Holleck, A. Kovács, P. Hovsepian, I. Gee, Constitution and microstructure of magnetron sputtered nanocomposite coatings in the system Ti–Al–N–C, Thin Solid Films 493 (2005) 104–112.
[5] S. Vepřek, S. Reiprich, S.Z. Li, Superhard nanocrystalline composite materials: the TiN/Si_3N_4 system, Appl. Phys. Lett. 66 (1995) 2640–2642.
[6] S. Vepřek, S. Reiprich, A concept for the design of novel superhard coatings, Thin Solid Films 268 (1995) 64–71.
[7] H. Gleiter, Nanostructured materials, Adv. Mater. 4 (1992) 474–481.
[8] S. Vepřek, M. Haussmann, S. Reiprich, S.Z. Li, J. Dian, Novel thermodynamically stable and oxidation resistant superhard coating materials, Surf. Coat. Technol. 86-87 (1996) 394–401.
[9] R.F. Zhang, A.S. Argon, S. Veprek, Friedel oscillations are limiting the strength of superhard nanocomposites and heterostructures, Phys. Rev. Lett. 102 (2009) 015503.
[10] L. Hultman, J. Bareño, A. Flink, H. Söderberg, K. Larsson, V. Petrova, M. Odén, J.E. Greene, I. Petrov, Interface structure in superhard TiN–SiN nanolaminates and nanocomposites: film growth experiments and ab initio calculations, Phys. Rev. B. 75 (2007) 155437.
[11] Q.M. Wang, K.H. Kim, Microstructural control of Cr–Si–N films by a hybrid arc ion plating and magnetron sputtering process, Acta Mater. 57 (2009) 4974–4987.
[12] J. Neidhardt, Z. Czigany, B. Satory, R. Tessadri, M. O'sullivan, C. Metterer, Nanocomposite Ti–B–N coatings synthesized by reactive arc evaporation, Acta Mater. 54 (2006) 4193–4200.
[13] Y. Sakamaoto, M. Nose, T. Mae, E. Honbo, M. Zhou, K. Nogi, Structure and properties of Cr–B, Cr–B–N and multilayer Cr–B/Cr–B–N thin films prepared by r.f.-sputtering, Surf. Coat. Technol. 174–175 (2003) 444–449.
[14] Y.H. Cheng, T. Browne, B. Heckerman, E.I. Meletis, Mechanical and tribological properties of nanocomposite TiSiN coatings, Surf. Coat. Technol. 204 (2010) 2123–2129.
[15] C.-L. Chang, C.-T. Lin, P.-C. Tsai, W.-Y. Ho, D.-Y. Wang, Influence of bias voltages on the structure and wear properties of TiSiN coating synthesized by cathodic arc plasma evaporation, Thin Solid Films 516 (2008) 5324–5329.
[16] N. Fateh, G.A. Fontalvo, G. Gassner, C. Mitterer, Influence of high-temperature oxide formation on the tribological behaviour of TiN and VN coatings, Wear 262 (2007) 1152–1158.
[17] R. Franz, C. Mitterer, Vanadium containing self-adaptive low-friction hard coatings for high-temperature applications: a review, Surf. Coat. Technol. 228 (2013) 1–13.
[18] F.F. Ge, P. Zhu, H.Y. Wang, F.P. Meng, S.Z. Li, F. Huang, Friction and wear behavior of magnetron co-sputtered V–Si–N coatings, Wear 315 (2014) 17–24.
[19] Y.T. Pei, P. Huizenga, D. Galvan, J.T.M. De Hosson, Breakdown of the Coulomb friction law in TiC/a-C:H nanocomposite coatings, J. Appl. Phys. 100 (2006) 114309.
[20] J. Shieh, M.H. Hon, Observation of plastic deformation in TiAlCN/aC ceramic nanocomposite coating, Appl. Phys. A Mater. Sci. Process. 80 (2005) 131–134.
[21] J. Musil, P. Zeman, H. Hrubý, ZrN/Cu nanocomposite film-a novel superhard material, Surf. Coat. Technol. 120-121 (1999) 179–183.
[22] F.P. Meng, B. Wang, F.F. Ge, F. Huang, Microstructure and mechanical properties of Ni-alloyed SiC coatings, Surf. Coat. Technol. 213 (2012) 77–83.
[23] A.A. Voevodin, J.S. Zabinski, Supertough wear-resistant coatings with 'chameleon' surface adaptation, Thin Solid Films 370 (2000) 223–231.
[24] J.C. Sánchez-López, D. Martínez-Martínez, C. López-Cartes, A. Fernández, Tribological behaviour of titanium carbide/amorphous carbon nanocomposite coatings: from macro to the micro-scale, Surf. Coat. Technol. 202 (2008) 4011–4018.
[25] R. Chen, J.P. Tu, D.G. Liu, Y.J. Mai, C.D. Gu, Microstructure, mechanical and tribological properties of TiCN nanocomposite films deposited by DC magnetron sputtering, Surf. Coat. Technol. 205 (2011) 5228–5234.
[26] T. Polcar, L. Cvrcek, P. Siroky, R. Novak, Tribological characteristics of CrCN coatings at elevated temperature, Vacuum 80 (2005) 113–116.
[27] L. Yate, L. Martínez-de-Olcoz, J. Esteve, A. Lousa, Effect of the bias voltage on the structure of nc-CrC/a-C:H coatings with high carbon content, Surf. Coat. Technol. 206 (2012) 2877–2883.
[28] H.J. Choe, S.H. Kwon, J.J. Lee, Tribological properties and thermal stability of TiAlCN coatings deposited by ICP-assisted sputtering, Surf. Coat. Technol. 228 (2013) 282–285.
[29] S.L. Ma, D.Y. Ma, Y. Guo, B. Xu, G.Z. Wu, K.W. Xu, P.K. Chu, Synthesis and characterization of super hard, self-lubricating Ti–Si–C–N nanocomposite coatings, Acta Mater. 55 (2007) 6350–6355.
[30] Q.S. Luo, S.C. Wang, Z.X. Zhou, L.H. Chen, Structure characterization and tribological study of magnetron sputtered nanocomposite nc-TiAlV(N,C)/a-C coatings, J. Mater. Chem. 21 (2011) 9746–9756.
[31] Z.Y. Wang, X.W. Li, J. Zhou, P. Liu, Q. Huang, P.L. Ke, A.Y. Wang, Microstructure evolution of V–Al–C coatings synthesized from a V2AlC compound target after vacuum annealing treatment, J. Alloys Compd. 661 (2016) 476–482.
[32] Y.Q. Zeng, Y.D. Qiu, X.Y. Mao, S.Y. Tan, Z. Tan, X.H. Zhang, J. Chen, J.Q. Jiang, Superhard TiAlCN coatings prepared by radio frequency magnetron sputtering, Thin Solid Films 584 (2015) 283–288.
[33] Z.L. Wu, J. Lin, J.J. Moore, M.K. Lei, Nanostructure transition in Cr–C–N coatings deposited by pulsed closed field unbalanced magnetron sputtering, Thin Solid Films 520 (2012) 4264–4269.
[34] J.L. Li, S.H. Zhang, M.X. Li, Influence of the C_2H_2 flow rate on gradient TiCN films deposited by multi-arc ion plating, Appl. Surf. Sci. 283 (2013) 134–144.
[35] W. Gulbinski, S. Mathur, H. Shen, T. Suszko, A. Gilewicz, B. Warcholinski, Evaluation of phase, composition, microstructure and properties in TiC/a-C:H thin films deposited by magnetron sputtering, Appl. Surf. Sci. 239 (2005) 302–310.
[36] L. Zhang, G.J. Ma, G.Q. Lin, H. Ma, K.C. Han, H.Y. Liu, Deposition and characterization of $Ti–C_x–N_y$ nanocomposite films by pulsed bias arc ion plating, Vacuum 106 (2014) 27–32.
[37] L. Escobar-Alarcona, V. Medina, E. Camps, S. Romero, M. Fernandez, D. Solis-Casados, Microstructural characterization of Ti–C–N thin films prepared by reactive crossed beam pulsed laser deposition, Appl. Surf. Sci. 257 (2011) 9033–9037.
[38] W. Dai, A.Y. Wang, Deposition and properties of Al-containing diamond-like carbon films by a hybrid ion beam sources, J. Alloys Compd. 509 (2011) 4626–4631.
[39] Y.H. Lu, Y.G. Shen, Nanostructure evolution and properties of two-phase nc-Ti(C,N)/a-(C, CN_x) nanocomposites by high-resolution transmission electron microscopy, x-ray photoelectron spectroscopy, and Raman spectroscopy, J. Mater. Res. 22 (2007) 2460–2469.
[40] J. Musil, Hard nanocomposite coatings: thermal stability, oxidation resistance and toughness, Surf. Coat. Technol. 207 (2012) 50–65.
[41] S. Zhang, H.L. Wang, S.-E. Ong, D. Sun, X.L. Bui, Hard yet tough nanocomposite coatings-present status and future trends, Plasma Process. Polym. 4 (2007) 219–228.
[42] O. Storz, H. Gasthuber, M. Woydt, Tribological properties of thermal-sprayed Magnéli-type coatings with different stoichiometries (Ti_nO_{2n-1}), Surf. Coat. Technol. 140 (2001) 76–81.